

Simultaneous measurement of charge carrier concentration, mobility, and lifetime



Dávid Krisztián ^{a,b,*}, Ferenc Korsós ^a, Gergely Havasi ^{a,b}

^a Semilab Co. Ltd., 2 Prielle K. str., 1117, Budapest, Hungary

^b Department of Physics, Institute of Physics, Budapest University of Technology and Economics, Műegyetem rkp. 3., H-1111, Budapest, Hungary

ARTICLE INFO

Keywords:

Carrier lifetime
Photoconductance decay
Carrier mobility
Characterization

ABSTRACT

For the first time, we have successfully combined the transient, steady-state, and small perturbation photoconductance decay lifetime measurement methods into a single system. The three operation modes complement each other and enhance the accuracy of each measurement, effectively compensating for the limitations of each individual mode. The goal is to provide very accurate carrier lifetime τ results as a function of injection level Δn over the entire illumination intensity range of interest for modern Si solar cells. The combination of the three methods not only results in mobility model-free $\tau(\Delta n)$ data with improved accuracy but provides the sum of the excess carrier mobilities as a function of Δn as well. This is important at high injection levels, where modern solar cells operate but mobility models in the literature exhibit significant differences.

The experimental setup developed for this purpose utilizes an eddy-current photoconductance sensor and lasers for the precise light control. Maintaining stable temperature for such measurements is a challenge that is overcome by applying smart laser control and advanced ventilation. The measurements yielded excellent agreement in the $\tau(\Delta n)$ values determined in the three fundamentally different modes and provided mobility values close to previously presented mobility models.

1. Introduction

Charge carrier recombination lifetime τ is a key parameter used to characterize crystalline silicon material and solar cell structures. It has several practical applications supporting solar cell development. Beyond the carrier lifetime as a single value, its injection level Δn dependence provides information identifying cell efficiency reducing recombination mechanisms, such as bulk defects [1,2], surface or p/n junction related phenomenon [3], or the recently revised intrinsic recombination limit [4,5].

In recent years, as a result of significantly improved surface passivation techniques [6], such as Si heterojunction techniques [7] or tunnel oxide-based routes [8,9], recombination losses have been drastically reduced, therefore τ and Δn reach very high levels in modern solar cell operation. This motivates us to explore the precision of the most commonly used carrier lifetime measurement methods and corresponding empirical models at these elevated injection levels.

The widely used Quasi-Steady-State Photoconductance (QSSPC) technique utilizes a flash lamp to generate electron-hole pairs in the sample and uses a radiofrequency (RF) coil to detect the conductivity

change $\Delta\sigma$ [10]. Δn is then calculated from $\Delta\sigma$ using an injection level dependent carrier mobility model $\mu(\Delta n)$. However, at high injection levels the most commonly employed mobility models exhibit considerable differences [11–13]. Furthermore, carrier mobility of non-standard wafer types (e.g. wafers from compensated silicon, kerfless manufacturing methods, casted ingots) can differ significantly from literature data.

Another well-established technique is the quasi-steady-state microwave detected photoconductance decay method (QSS-μPCD) [14]. It applies continuous laser illumination to develop a steady state condition while the so-called differential or small perturbation lifetime τ_d is probed at each steady state level using a second laser emitting weak photon pulses. In this paper, this method is referred to as the small perturbation photoconductance decay method (SP-PCD). The actual lifetime and injection level can be determined using this technique as well [15] but without using $\mu(\Delta n)$ models. On the other hand, optical losses should be precisely known to determine an accurate injection level.

The charge carrier mobility in monocrystalline silicon has been calculated in several earlier studies as a function of the doping concentration and temperature [16,17]. Although solar cells typically

* Corresponding author. Semilab Co. Ltd., 4/A Prielle K. str., 1117, Budapest, Hungary.

E-mail address: david.krisztian@semilab.hu (D. Krisztián).

operate at high injection levels, only a few experimental studies discuss the injection level dependence of the mobility. Both semi-empirical models [11,12] and experimental models are widely known. In the most often used experimental dataset, Dannhauser [18] and Krausse [19] employ the voltage measurement of pn-junctions to obtain $\mu(\Delta n)$. In the last two decades, three major photoconductance measurement based works were presented for the same purpose. Neuhaus et al. used the quasi-steady-state open circuit voltage method (QSS-Voc) [20], Rougieux et al. presented a contactless method combining the transient and the steady state lifetime measurement of the QSSPC technique using samples in an intermediate carrier lifetime range [21]. Finally, Hameiri et al. determined the Δn using an independently calibrated photoluminescence measurement [22].

In this study, we present a photoconductance based experimental setup, which integrates transient photoconductance (transient PC), steady state PC (SS-PC) and SP-PCD lifetime measurement techniques using laser illumination. Since the SP-PCD method provides a mobility-free injection level calculation, this combined technique enables the determination of $\mu(\Delta n)$ in a new contactless way, avoiding all limitations of the previous similar approaches.

2. Methods

2.1. Carrier lifetime measurement methods

As pointed out in the introduction, our measurement setup developed for the unified lifetime measurement integrates the three main photoconductance based carrier lifetime measurement principles, which are available in different commercial and experimental measurement systems.

In the photoconductance decay (PCD) technique, the primary measured quantity is the sheet conductance σ_{sh} of the illuminated sample. The σ_{sh} measurement can be obtained using a contact resistance measurement or by contactless sensors applying electromagnetic waves at different frequencies (e.g. infrared light absorption, microwave or radiofrequency sensors [23]). Accurate σ_{sh} data is obtained using a calibrated radiofrequency (RF) sensor in commercial systems, such as QSSPC or eddy-current PCD (ePCD) [24].

In the very general case, the excess carrier distribution is not uniform in either depth (z) or laterally (r), and its shape also varies during the photoconductance decay measurement. For the proper evaluation of the recorded decay curves, this inhomogeneity phenomenon should be considered. However, if the diffusion length of the excess carriers exceeds the wafer thickness significantly and the surface passivation is sufficient, $\Delta n(z)$ is uniform enough to not limit the accuracy of the derived carrier lifetime. This is true for all three lifetime measurement methods. For the experimental platform we used in this work [25], our simulations and experimental results proved that it applies a sufficiently large and uniform illumination to provide lifetime accuracy within 1% in the entire range of interest without considering the possible variation of $\Delta n(r)$.

In this study, we used thin Si wafers with a reasonably long bulk lifetime and decent passivation, therefore $\Delta n(z, r)$ is homogenous enough to ensure the validity of the basic carrier lifetime formulas relating to the change of the average carrier concentration $\Delta n(t)$ and to avoid the effect of carrier diffusion related phenomena. We will use this simplification throughout the discussion.

2.1.1. Methods requiring a mobility model: transient PC and SS-PC

The injection level can be calculated iteratively using the wafer thickness W and a $\mu(\Delta n)$ model (Eq. (1).):

$$\Delta n = \frac{\sigma_{sh}}{W \cdot e \cdot \mu(\Delta n)}. \quad (1)$$

The applied light source is an important factor in choosing the proper lifetime evaluation method. After the illumination is completely

terminated, the transient PC evaluation method is applicable, and the lifetime can be calculated from the decay rate of excess carriers (Eq. (2).):

$$\tau = \frac{\Delta n}{\frac{d\Delta n}{dt}}. \quad (2)$$

This evaluation method can be used in laser-based PCD tools [24] or in flash-lamp systems when the carrier lifetime is longer than the decay time of the illumination.

If using a continuous light source, or if the decay time of the light source significantly exceeds the carrier lifetime τ , the pure steady-state evaluation (SS-PC) is applicable (Eq. (3).):

$$\tau = \frac{\Delta n}{G_{ss}}, \quad (3)$$

where generation rate G_{ss} must be precisely known. In theory, if using a controlled laser light source both methods can be realized separately, while using flash-lamp-based systems in a given carrier lifetime range, the so-called generalized or quasi-steady-state (QSS) evaluation must be used (Eq. (4).):

$$\tau = \frac{\Delta n}{G_{ss} - \frac{d\Delta n}{dt}}. \quad (4)$$

2.1.2. Small-perturbation method: SP-PCD

While both the transient PC and SS-PC methods require calibration of the sheet conductance sensor and a mobility model to convert σ_{sh} into Δn , small perturbation methods do not use these data. As it is explained in Refs. [14,15], if the change of Δn (generated by the perturbing light source) is small enough during the differential lifetime τ_d sampling compared to the steady-state light source related carrier density $\Delta n(G_{ss})$, the variation of mobility during the τ_d sampling can be neglected. Since τ_d corresponding to a given steady-state generation rate is determined from a single exponential fit of the signal decay after switching the perturbing laser off, the τ_d value does not rely on a mobility model or PC sensor calibration.

Furthermore, the actual lifetime and injection level can be determined by recording τ_d as a function of the steady state illumination level:

$$\tau(G_{ss}) = \frac{1}{G_{ss}} \int_0^{G_{ss}} \tau_d(G'_{ss}) dG'_{ss}, \quad (5)$$

$$\Delta n(G_{ss}) = G_{ss} \cdot \tau(G_{ss}). \quad (6)$$

The optical properties of the sample must be known for the determination of generation rate G_{ss} . It is typically determined using an optical factor OF as the ratio of absorbed photons to all incident ones.

We introduced an earlier version of our experimental setup in Ref. [25], which combined the transient PC and SP-PCD techniques complementing each other in terms of practical advantages and disadvantages. The transient PC method is considered accurate at low injection levels, where mobility models agree well, while SP-PCD is more reliable at higher injection levels. Now we present further improvements which enable the integration of the third available method, SS-PC, into our setup as well.

2.2. Setup and measurement procedure

A schematic illustration of the measurement setup we developed for the multi-method carrier lifetime measurement is depicted in Fig. 1. A high power 915 nm continuous wave (CW) laser is used as the steady state light source for SS-PC and SP-PCD, while a 980 nm modulated CW laser acts as the light source for the transient PC measurement as well as the “small perturbation” illumination source with reduced power for SP-PCD. The 3 cm diameter illumination spot of both laser beams are very homogenous to avoid lateral diffusion effects. The eddy current sensor

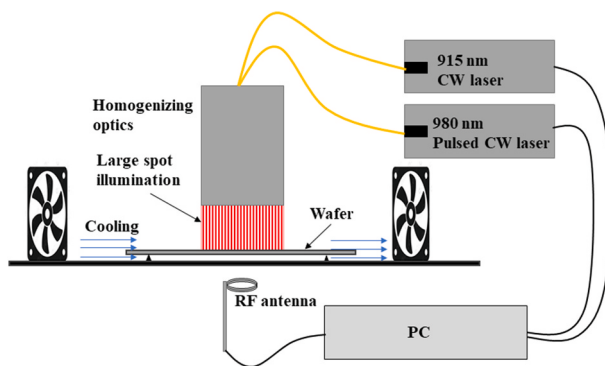


Fig. 1. The schematic drawing of the integrated carrier lifetime measurement setup. Large spot illumination is applied to avoid lateral diffusion phenomena. Continuous cooling is applied to reduce sample warming during the high intensity illumination.

consists of an RF coil with 13 mm diameter. The description of the electrical and optical components of the setup is detailed in Ref. [25].

Recently, Black et al. [26], proposed a complex method for the precise σ_{sh} calibration of the RF sensor, pointing out that the thickness of calibrating samples and their distance to the coil must be considered. Instead, we applied a much simpler approach. We used sheet resistance calibration wafers of very similar thickness to what was used for the measurement.

We simultaneously performed the steady-state and small perturbation measurements within one sequential measurement cycle as illustrated in Fig. 2a and b. The high intensity laser is switched on first with a generation rate $G_{ss,1}$, and the steady state photoconductance σ_{ss} data is recorded when the signal is already saturated. Then the τ_d sampling small intensity light pulse ($G_{p,1}$) is applied. This measurement sequence is repeated at different steady-state excitation levels to acquire $\sigma_{ss}(G_{ss})$ and $\tau_d(G_{ss})$ plots.

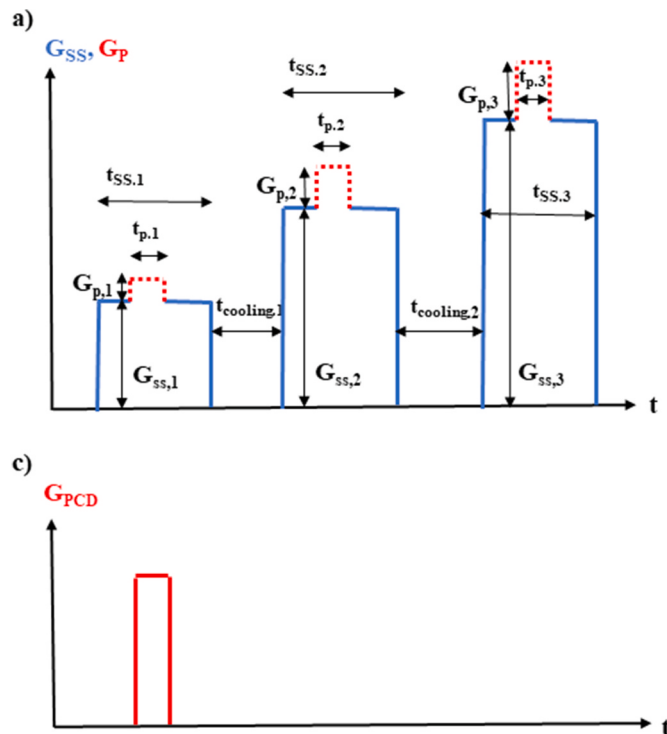


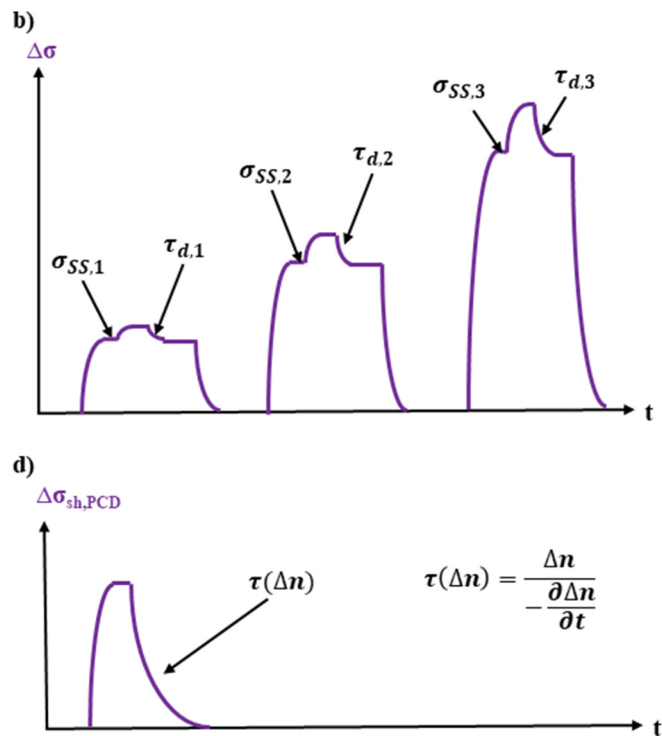
Fig. 2. The illustration of the SP-PCD and SS-PC measurement sequence explaining (a) how the two lasers are applied and (b) how the excess sheet conductance changes during the measurement procedure to obtain $\sigma_{ss}(G_{ss})$ and $\tau_d(G_{ss})$ plots. The transient PC measurement is performed individually using the same modulated 980 nm laser functioning as the τ_d probing laser for SP-PCD (c) just with larger intensity. Then the $\tau_{PCD}(\Delta n)$ is calculated from the decay of the measured sheet conductance (d).

The rapid transient PC measurement is performed individually after the SS-PCD and SP-PCD combined measurement, as shown in Fig. 2c and d.

We applied high illumination intensity (up to ~ 40 Suns) to analyze the samples in the high injection regime, which caused significant sample warming during the steady state measurements. The wafer can warm up by tens of degrees (Fig. 3a.) when continuously illuminated with the steady state light. In the case of such a significant temperature rise, the mobility is changing significantly, so the evaluation in general would be very problematic. Therefore, to reduce the warming in two independent ways, we applied an advanced ventilation technique (Fig. 1.) and used smart control of the SS laser. After each τ_d sampling, it was switched off for a given period ($t_{cooling}$) adjusted according to the applied intensity (G_{ss}) and length (t_{ss}) of the steady state light pulse (Fig. 2a.). In this way, we managed to keep the temperature variation of the sample below 4°C during the measurement even at very high light intensities (Fig. 3b.).

2.3. Samples

Several wafers were measured using the described methods to demonstrate the capability of the integrated system. To demonstrate the method, results from 150 μm thick textured phosphorus doped n-type and gallium doped p-type Czochralski-grown mono-Si wafers are reported. Both types were passivated with a stack of intrinsic and doped hydrogenated amorphous silicon layers (a-Si:H) deposited using PE-CVD. N-type and p-type a-Si:H layers were deposited symmetrically on each side of the n-type and p-type wafers, respectively. A transparent conductive oxide layer (typical conducting layer in Si heterojunction cell technique) was not deposited to directly measure the sheet conductance of the bulk crystalline silicon. In the presented high lifetime samples charge carrier trapping is not observable at room temperature, which allows us to assume identical excess hole and electron concentration.



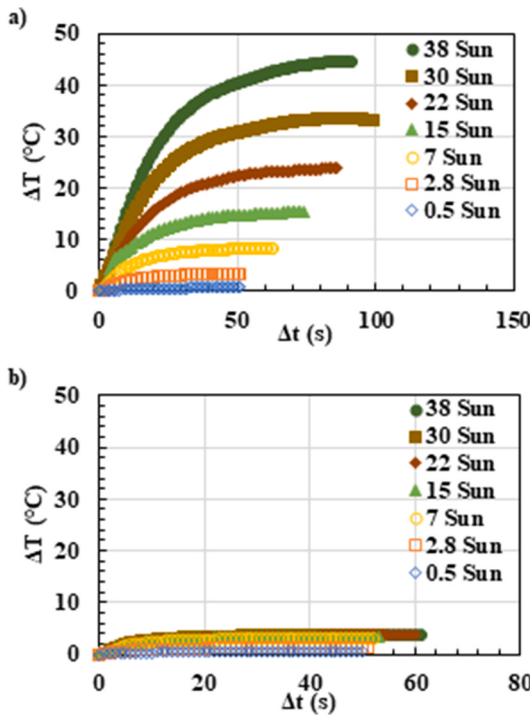


Fig. 3. Temperature rise during the steady state measurement procedure at different illumination intensities (a) without cooling and (b) after applying ventilation and smart SS laser control.

3. Unification of transient PC, SS-PC and SP-PCD methods

In the previous section, we summarized the basic carrier lifetime measurement methods, and presented the physical realization of their integration into one experimental setup. Now we discuss how these methods can mutually improve each other in terms of accuracy by providing physical parameters for the other method, which finally leads to the determination of carrier mobility from this unified protocol.

3.1. Optical factor for SP-PCD and SS-PC

A precise optical factor data is required to calculate G_{ss} from the light intensity, which is typically determined by optical measurements. However, we can obtain more accurate data using the integrated setup. Since the transient PC measurement is detected with the same calibrated sensor, the measured σ_{sh} corresponds to the same injection level and generation rate independent from the actual measurement method. A so-called implied generation rate $G_{imp}(\Delta n) = -\partial \Delta n / \partial t$ can be derived by evaluating the transient PC decay. This should give the same generation rate as the steady state light source G_{ss} which physically produces the same σ_{sh} . Therefore, if we suppose that in some injection level regimes the individual transient PC measurement is accurate enough, the precision of the optical factor can be enhanced by taking the ratio of G_{imp} and the steady state photon current density J_{ph} (for the SP-PCD and SS-PC measurements) corresponding to the same sheet conductance (signal level). So:

$$OF = \frac{G_{imp}(\Delta n)}{J_{ph}(\Delta n)} \Big|_{\sigma_{sh, tr-PC} = \sigma_{sh, SS}(G_{ss})}. \quad (7)$$

Since the G_{imp} value in Eq. (7) depends on mobility model, we make this adjustment at a suitably low injection level, where the $\mu(\Delta n)$ mobility models agree well and are therefore considered reliable. In Fig. 5a. we present an example of the OF determination.

3.2. Enhancement of the accuracy of SP-PCD by actual lifetime matching at low injection levels

As shown by Wilson et al. [14], in order to obtain an accurate τ_d result at a given steady state injection level, the perturbing laser power (G_p) must be sufficiently low compared to the steady state light source. This ensures the small perturbation nature of the measurement, which results in transient curves with pure exponentiality and indicates the reliability of the recorded τ_d value. If a larger G_p is used, the measured τ_d becomes inaccurate, since the injection level changes significantly during the measurement, therefore the small perturbation requirement is not maintained.

On the other hand, applying too low of a G_p results in a low measurement signal and high noise which makes it complicated and very time-consuming to obtain a reliable τ_d . Therefore, for each G_{ss} level, we need to define an optimal G_p range which provides an accurate τ_d value with a tolerable noise in a reasonable measurement time (Fig. 4.). We determined this optimal G_p range using different samples and several G_{ss} levels, and finally defined a very simple rule that in almost all cases, this optimal G_p range was around 10–20% of the G_{ss} . Therefore, to be on the safe side in terms of accuracy, for all τ_d samplings we used a 10% G_p/G_{ss} ratio during the SP-PCD measurement. As it is demonstrated in Fig. 5b., under this SP-PCD condition, the recorded SP-PCD transient is indeed purely exponential.

The smallest steady-state laser intensity where such an accurate SP-PCD measurement can be performed determines the initial point of the small perturbation method evaluation ($G_{ss,1}$). However, the actual lifetime at this injection level (τ_1) is undefined and may reduce the precision of the actual lifetimes at higher injections as well due to the integrated calculation of τ . Again, τ_1 can be taken from the transient PC measurement at the same sheet conductance level by supposing that (Eq. (8).):

$$\tau_1 = \tau_{tr-PC} \Big|_{\sigma_{sh, tr-PC} = \sigma_{sh, SS}(G_{ss,1})}, \quad (8)$$

so actually matching them at the same signal levels (Fig. 5c and d.). At each steady-state illumination level over $G_{ss,1}$, the actual lifetime is calculated by numerical integration of τ_d applying Eq. (5). for a finite number of measurement points:

$$\tau_{SP}(G_{ss}) = \tau_1 + \frac{1}{G_{ss} - G_{ss,1}} \sum_{i=1}^{G_{ss}} \tau_d(G_{ss}^i) \cdot (G_{ss}^i - G_{ss}^{i-1}). \quad (9)$$

Using the actual lifetime value from Eq. (9)., the accurate injection level can be calculated over $1e15 \text{ cm}^{-3}$ using Eq. (6). (see the result in Fig. 5e.). In the case of samples with lower carrier lifetime, the validity interval of the SP-PCD measurement shifts to lower values, since the $\Delta n(G_{ss,1})$ is lower.

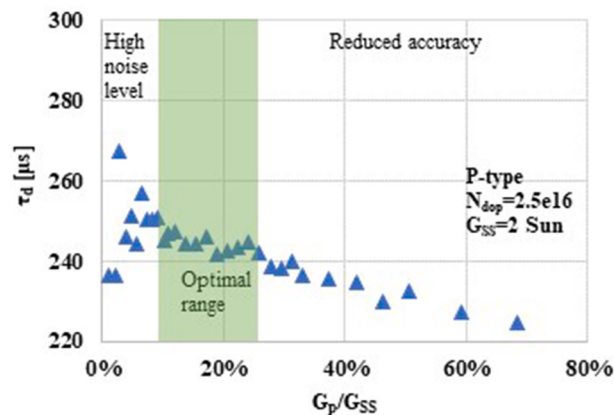


Fig. 4. Measured differential lifetime as a function of the probing laser power. 10–20% of the SS laser intensity was found to be the optimal range where the results are accurate yet not noisy.

In the previous two subsections we have shown how the transient PC method can be used to improve the accuracy of SP-PCD measurement by matching generation rate and lifetime at the same signal level. Each step of the calculation of $\tau(\Delta n)$ using the SP-PCD method following our approach is demonstrated by the measurements summarized in Fig. 5.

3.3. Mobility determination

The combination of SS-PC and SP-PCD methods can provide information about the mobility of the excess carriers. Following the SP-PCD measurement sequence illustrated in Fig. 2, one can record $\Delta n(G_{ss})$ without using mobility models for the high injection level regime. Additionally, as shown in Fig. 2b, the sheet conductance (and so the conductivity $\sigma(G_{ss})$) can be recorded simultaneously. Therefore the $\sigma(\Delta n)$ can be easily constructed. From this purely experimental relationship, the sum of excess minority and majority mobilities $\mu_{sum}(\Delta n)$

can be calculated as follows.

In previous similar studies [20–22] $\mu_{sum}(\Delta n)$ was estimated as the ratio of excess conductivity and the injection level (Eq. (10).):

$$\mu_{sum}(\Delta n, N_{dop}) = \frac{\Delta\sigma}{e \cdot \Delta n}. \quad (10)$$

However, it has been recently shown that the correct formula of $\sigma(\Delta n)$ must consider the mobility shift of majority carriers [4]:

$$\sigma = e \cdot (\mu_{sum}(N_{dop}, \Delta n) \cdot \Delta n + \mu_{maj}(N_{dop}, \Delta n) \cdot N_{dop}). \quad (11)$$

Eq. (11), includes both μ_{sum} and the majority carrier mobility μ_{maj} . Unfortunately, the conductance of electrons and holes cannot be separated using photoconductance based measurements. To overcome this challenge, we introduced the ratio of electron and hole mobilities $f(N_{dop}, \Delta n) = \mu_h(N_{dop}, \Delta n) / \mu_p(N_{dop}, \Delta n)$, and expressed μ_{sum} from the measured $\sigma(\Delta n)$ curve using $f(N_{dop}, \Delta n)$ for p-type samples:

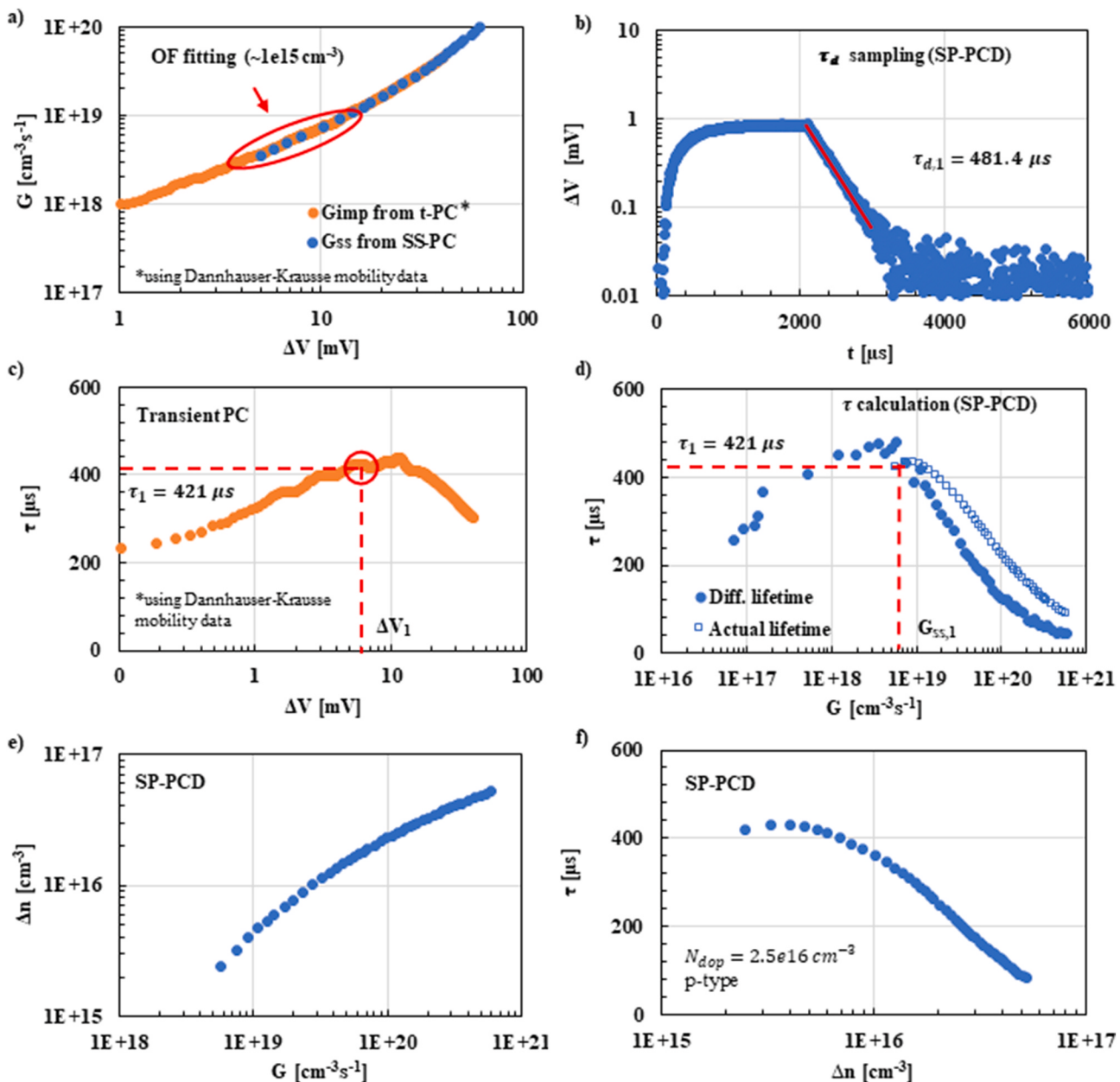


Fig. 5. Evaluation of SP-PCD measurement step-by-step. (a) Optical factor is determined by generation rate matching with transient PC. (b) Under the appropriate excitation level, a pure exponential curve is measured by small perturbation. (c–d) The initial actual lifetime τ_1 is determined from the transient PC measurement as well. (e–f) accurate injection level and actual lifetime values are obtained over $1e15 \text{ cm}^{-3}$.

$$\mu_{sum}(\Delta n, N_{dop}) = \frac{\sigma}{e \cdot \left(\Delta n + \frac{1}{1+f(N_{dop}, \Delta n)} N_{dop} \right)}. \quad (12)$$

For n-type samples the inverse of the f value has to be used in the formula. We estimated the $f(N_{dop}, \Delta n)$ factor in two different ways. First, without using any theoretical mobility models, assuming that $f = 2.25$ which is equal to the ratio of effective masses of electrons and holes (using the effective mass values used for the calculation of density of states [27]). Second, using the semi-empirical mobility model proposed by Klaassen [12]. This latter approach is supported by mobility models, however, μ_n , μ_p values from the Klaassen model are not used directly, only their ratio is taken (Fig. 6a.) and used only for the proper compensation of the shift of the conductivity originating from doping atoms (" σ_0 shift") in the excited samples. The mobility results computed using Eq. (12), and applying the two $f(N_{dop}, \Delta n)$ calculation principles are plotted in Fig. 6b. corresponding to the same p-type sample used in acquiring carrier lifetime results in Fig. 5. Compared to the case if the σ_0 shift is not considered, the compensation of this phenomenon results in a 2–5% μ_{sum} increase assuming a constant f factor, while a further 3% increase is observed using the Klaassen model based correction, mainly at lower injection levels, where the actual f value is far from $\mu_n/\mu_p = 2.25$.

To summarize how the three lifetime evaluation methods complement and support each other, finally leading to the calculation of the mobility sum, we constructed a Venn-diagram illustrating the used methods and formulas (Fig. 7.).

Please note that our mobility calculation method is only applicable in the case of ordinary recombination processes where carrier trapping phenomena are not significant. In some PV materials carrier trapping can result in improperly long evaluated lifetimes from the PCD measurement, especially in the low injection regime. In this case the PCD transient does not follow the recombination described by the actual lifetime and therefore our method is not applicable. The monocrystalline samples we used for the experiments do not exhibit perceptible trapping behavior and are therefore perfectly suitable to accurately obtain the carrier mobility.

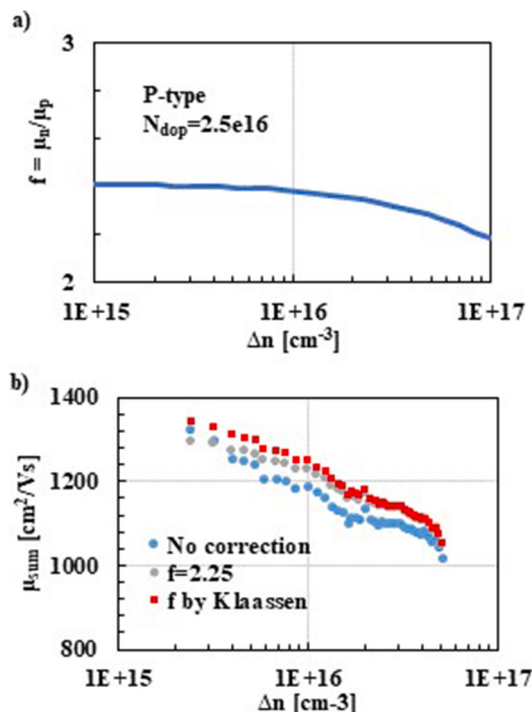


Fig. 6. (a) The ratio of μ_n and μ_p using the parametrization of Klaassen [12]. (b) μ_{sum} (Δn) measured by the multi-method carrier lifetime technique.

4. Proof of concept results

We measured several different samples using the described method. To illustrate the capabilities of the integrated system, we selected results obtained from a-Si:H passivated p- and n-type mono-Si wafers. In Fig. 8a and b. the carrier lifetime results of the SP-PCD method are compared to the result of the original transient PC and the SS-PC method. For the evaluation of these two latter methods, the parametrization of the most widely used Dannhauser-Krausse mobility data [18,19] is applied. The sum of electron and hole mobilities is depicted on Fig. 8c and d. as a function of the injection level. These $\mu_{sum}(\Delta n)$ results are compared to the most commonly used mobility models for lifetime measurements at room temperature (298 K). Our experimental mobility results from the "ideal" mono-Si p and n-type wafers are very close to the Dannhauser-Krausse model even at high injection levels. The minor deviations between the mobility values are responsible for the slight differences between SP-PCD and SS-PC lifetimes in Fig. 8a and b.

From the results, we can conclude that the great matching of lifetime results by the three lifetime measurement methods and the mobility results closely matching to existing models further confirm the reliability of the measurement setup and the presented combined technique.

We also compared the measured $\mu_{sum}(\Delta n)$ curves to the model of Zheng et al. [13], who used an experimental dataset determined by a similar combined carrier lifetime approach using samples from a given carrier lifetime range employing a flash-lamp system in its QSS and transient PC modes. Beyond the observation that our results are closer to other literature data, the presented laser based photoconductance measuring routine can be applied more universally to practically any typical modern PV wafer.

5. Conclusions

We presented a carrier lifetime measurement setup, which integrates three different lifetime measurement principles: transient PC, SS-PC and SP-PCD. This combination enables the determination of carrier lifetime, injection level, and mobility in silicon samples typically used in state-of-the-art solar cells. We achieved excellent agreement between the lifetime and injection level results obtained from the three methods using the parametrization of Dannhauser-Krausse mobility data for PC measurements. Furthermore, the mobility results from standard mono-Si wafers are quite close to the prediction of previously published mobility models at room temperature. The combination of these facts serves to validate the reliability of the unified method. This measurement technique and platform facilitate precise and comprehensive characterization of non-standard wafer types (e.g. wafers from different casting methods or compensated silicon), where current models may be inadequate.

CRediT authorship contribution statement

Dávid Krisztián: Writing – original draft, Visualization, Validation, Software, Methodology, Investigation, Formal analysis, Data curation. **Ferenc Korsós:** Writing – original draft, Supervision, Methodology, Formal analysis, Conceptualization. **Gergely Havasi:** Data curation.

Declaration of competing interest

The authors declare that they have no known competing financial interests or personal relationships that could have appeared to influence the work reported in this paper.

Data availability

Data will be made available on request.

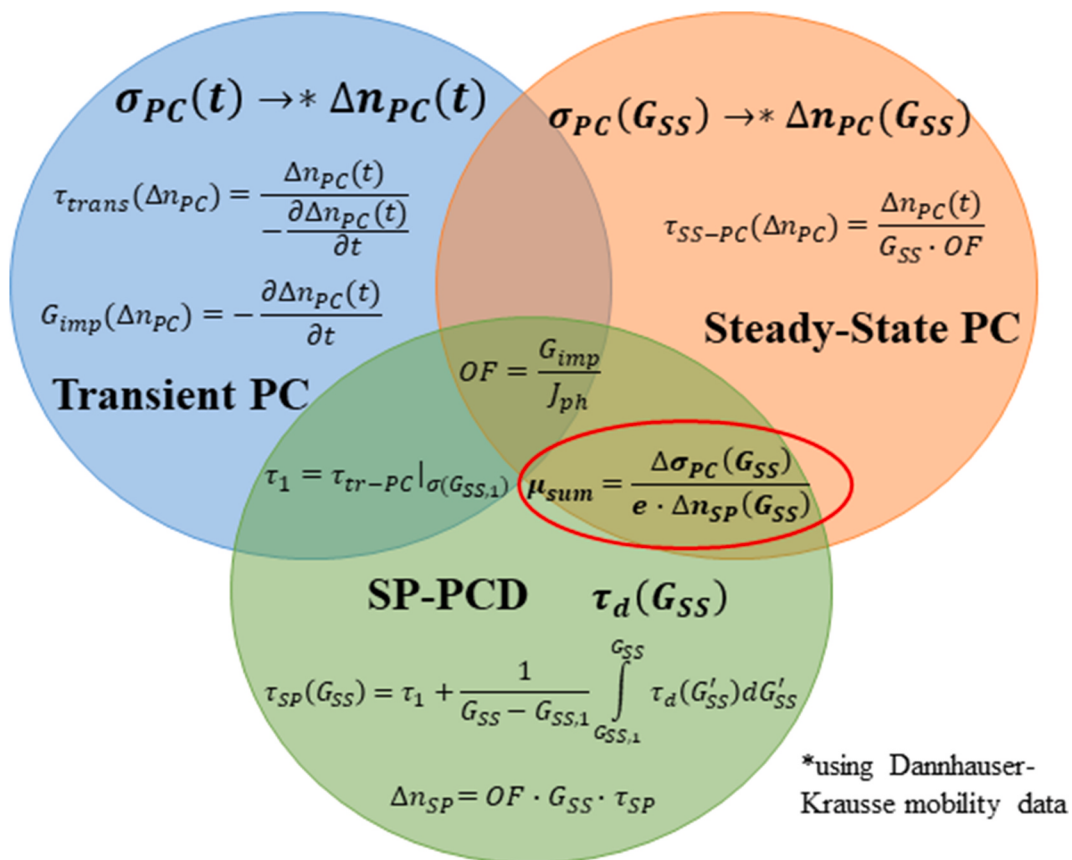


Fig. 7. The Venn-diagram summarizes the applied carrier lifetimes methods and formulas used to determine the mobility sum.

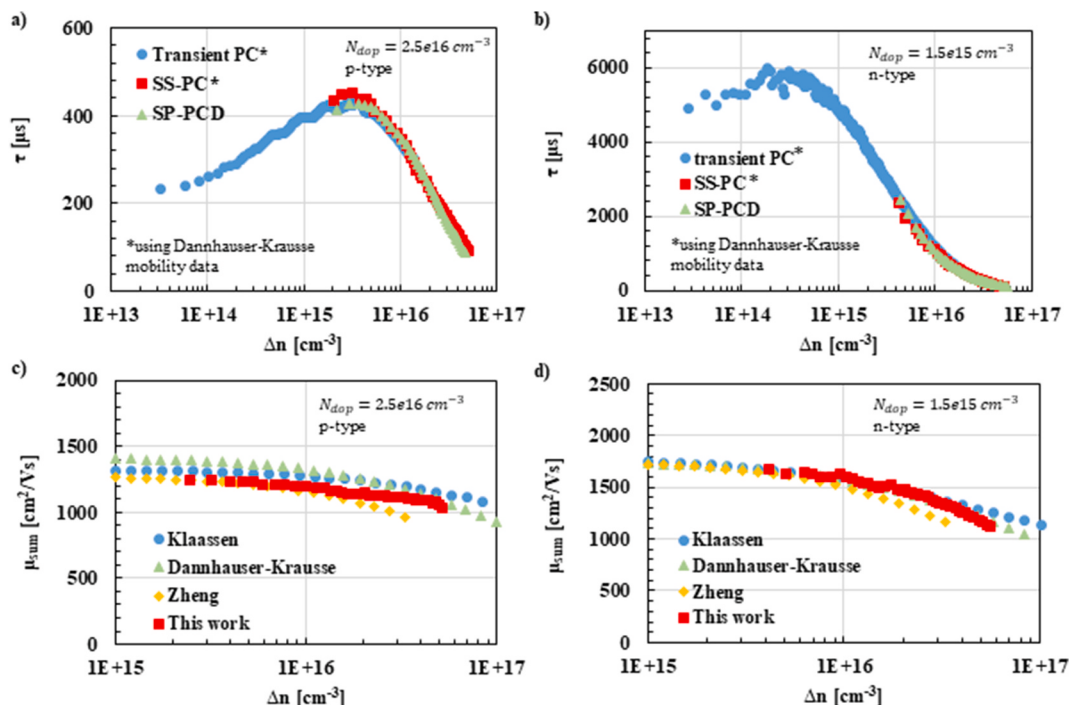


Fig. 8. The $\tau(\Delta n)$ obtained by three different lifetime techniques agrees well even at high injection levels for both the p-type (a) and n-type (b) samples. (c-d) The derived $\mu_{sum}(\Delta n)$ for both wafers is close to the experimental model proposed by Dannhauser and Krausse. Sample details in section 2.3.

Acknowledgements

We thank Marshall Wilson for useful discussions. Project no. C1010858 has been implemented with the support provided by the Ministry of Culture and Innovation of Hungary from the National Research, Development and Innovation Fund, financed under the KDP-2020 funding scheme.

Appendix A. Supplementary data

Supplementary data to this article can be found online at <https://doi.org/10.1016/j.solmat.2023.112461>.

References

- [1] J.D. Murphy, M. Al-Amin, K. Bothe, M. Olmo, V.V. Voronkov, R.J. Falster, The effect of oxide precipitates on minority carrier lifetime in n-type silicon, *J. Appl. Phys.* 118 (2015), 215706, <https://doi.org/10.1063/1.4936852>.
- [2] F. Korsós, L. Roszol, F. Jay, J. Veirman, A.D. Draoua, M. Albaric, T. Szarvas, Z. Kiss, A. Szabó, I. Soczó, Gy Nádudvari, N. Laurent, Efficiency limiting crystal defects in monocrystalline silicon and their characterization in production, *Sol. Energy Mater. Sol. Cell.* 186 (2018) 217–226, <https://doi.org/10.1016/j.solmat.2018.06.030>.
- [3] D.E. Kane, R.M. Swanson, Measurement of the emitter saturation current by a contactless photoconductivity decay method, in: Proc. IEEE 18th Photovoltaic Specialist Conf., 1985, p. 578.
- [4] L.E. Black, D.H. Macdonald, On the quantification of Auger recombination in crystalline silicon, *Sol. Energy Mater. Sol. Cell.* 234 (2022), 111428, <https://doi.org/10.1016/j.solmat.2021.111428>.
- [5] T. Niewelt, B. Steinhauser, A. Richter, B. Veith-Wolf, A. Fell, B. Hammann, N. E. Grant, L. Black, J. Tan, A. Youssef, J.D. Murphy, J. Schmidt, M.C. Schubert, S. W. Glunz, Reassessment of the intrinsic bulk recombination in crystalline silicon, *Sol. Energy Mater. Sol. Cell.* 235 (2022), 111467, <https://doi.org/10.1016/j.solmat.2021.111467>.
- [6] 14th Edition of International Technology Roadmap for Photovoltaic (IRTPV), 2023.
- [7] K. Yoshikawa, H. Kawasaki, W. Yoshida, et al., Silicon heterojunction solar cell with interdigitated back contacts for a photoconversion efficiency over 26%, *Nat. Energy* 2 (2017), 17032 <https://doi.org/10.1038/nenergy.2017.32>.
- [8] F. Feldmann, M. Bivour, C. Reichel, H. Steinkeper, M. Hermle, S.W. Glunz, Tunnel oxide passivated contacts as an alternative to partial rear contacts, *Sol. Energy Mater. Sol. Cell.* 131 (2014) 46–50, <https://doi.org/10.1016/j.solmat.2014.06.015>.
- [9] F. Haase, C. Hollemann, S. Schäfer, A. Merkle, M. Rienäcker, J. Krügener, R. Brendel, R. Peibst, Laser contact openings for local poly-Si-metal contacts enabling 26.1%-efficient POLO-IBC solar cells, *Sol. Energy Mater. Sol. Cell.* 186 (2018) 184–193, <https://doi.org/10.1016/j.solmat.2018.06.020>.
- [10] R.A. Sinton, A. Cuevas, M. Stuckings, Quasi-steady-state photoconductance, a new method for solar cell material and device characterization, in: Conference Record of the Twenty Fifth IEEE Photovoltaic Specialists Conference - 1996, 1996, pp. 457–460, <https://doi.org/10.1109/PVSC.1996.564042>. Washington, DC, USA.
- [11] J.M. Dorkel, Ph Leturcq, Carrier mobilities in silicon semi-empirically related to temperature, doping and injection level, *Solid State Electron.* 24 (1981) 821–825, [https://doi.org/10.1016/0038-1101\(81\)90097-6](https://doi.org/10.1016/0038-1101(81)90097-6).
- [12] D.B.M. Klaassen, A unified mobility model for device simulation—I. Model equations and concentration dependence, *Solid State Electron.* 35 (1992) 953–959, [https://doi.org/10.1016/0038-1101\(92\)90325-7](https://doi.org/10.1016/0038-1101(92)90325-7).
- [13] P. Zheng, F.E. Rougieux, D. Macdonald, A. Cuevas, Measurement and parameterization of carrier mobility sum in silicon as a function of doping, temperature and injection level, *IEEE J. Photovoltaics* 4 (2014) 560–565, <https://doi.org/10.1109/JPHOTOV.2013.2294755>.
- [14] M. Wilson, P. Edelman, J. Lagowski, S. Olibet, V. Mihaileti, Improved QSS-μPCD measurement with quality of decay control: correlation with steady-state carrier lifetime, *Sol. Energy Mater. Sol. Cell.* 106 (2012) 66–70, <https://doi.org/10.1016/j.solmat.2012.05.040>.
- [15] J. Schmidt, Measurement of differential and actual recombination parameters on crystalline silicon wafers [solar cells], *IEEE Trans. Electron. Dev.* 46 (1999) 2018–2025, <https://doi.org/10.1109/16.791991>.
- [16] G. Masetti, M. Severi, S. Solmi, Modeling of carrier mobility against carrier concentration in arsenic-, phosphorus-, and boron-doped silicon, *IEEE Trans. Electron. Dev.* 30 (1983) 764–769, <https://doi.org/10.1109/T-ED.1983.21207>.
- [17] F. Schindler, M.C. Schubert, A. Kimmerle, J. Broisch, S. Rein, W. Kwapił, W. Warta, Modeling majority carrier mobility in compensated crystalline silicon for solar cells, *Sol. Energy Mater. Sol. Cell.* 106 (2012) 31–36, <https://doi.org/10.1016/j.solmat.2012.06.018>.
- [18] F. Dannhäuser, Die abhängigkeit der trägerbeweglichkeit in silizium von der konzentration der freien ladungsträger—I, *Solid State Electron.* 15 (1972) 1371–1375, [https://doi.org/10.1016/0038-1101\(72\)90131-1](https://doi.org/10.1016/0038-1101(72)90131-1).
- [19] J. Krausse, Die abhängigkeit der trägerbeweglichkeit in silizium von der konzentration der freien ladungsträger—II, *Solid State Electron.* 15 (1972) 1377–1381, [https://doi.org/10.1016/0038-1101\(72\)90132-3](https://doi.org/10.1016/0038-1101(72)90132-3).
- [20] D. Neuhaus, P. Altermatt, A. Sproul, R. Sinton, A. Schenk, A. Wang, A. Aberle, Method for measuring minority and majority carrier mobilities in solar cells, in: Proceedings of the 17th European Photovoltaic Solar Energy Conference, 2001, pp. 242–245.
- [21] F.E. Rougieux, P. Zheng, M. Thiboust, J. Tan, N.E. Grant, D.H. Macdonald, A. Cuevas, A contactless method for determining the carrier mobility sum in silicon wafers, *IEEE J. Photovoltaics* 2 (2012) 41–46, <https://doi.org/10.1109/JPHOTOV.2011.2175705>.
- [22] Z. Hameiri, F. Rougieux, R. Sinton, T. Trupke, Contactless determination of the carrier mobility sum in silicon wafers using combined photoluminescence and photoconductance measurements, *Appl. Phys. Lett.* 104 (2014), 073506, <https://doi.org/10.1063/1.4865804>.
- [23] D.K. Schroder, Carrier lifetimes, in: *Semiconductor Material and Device Characterization*, Wiley-IEEE Press, 2006, pp. 389–464.
- [24] D. Krisztián, F. Korsós, I. Saegh, G. Paráda, M. Kovács, Z. Verdon, Cs Jobbág, P. Tüttö, X. Dong, H. Deng, S. Wang, X. Chen, Improved accuracy of eddy-current sensor based carrier lifetime measurement using laser excitation, *EPJ Photovolt* 13 (2022) 3, <https://doi.org/10.1051/epjpv/2021014>.
- [25] D. Krisztián, F. Korsós, E. Kis, G. Paráda, P. Tüttö, Integrated measurement of the actual and small perturbation lifetimes with improved accuracy, in: *AIP Conference Proceedings of SiliconPV*, 2022 (in press).
- [26] L.E. Black, D.H. Macdonald, Accounting for the dependence of coil sensitivity on sample thickness and lift-off in inductively coupled photoconductance measurements, *IEEE J. Photovoltaics* 9 (6) (2019) 1563–1574, <https://doi.org/10.1109/JPHOTOV.2019.2942484>.
- [27] <http://www.ioffe.ru/SVA/NSM/Semicond/Si/bandstr.html#Masses>. (Accessed 26 June 2023).